Underwater Acoustic Communication Using Multiple-Input Multiple-Output Doppler-Resilient Orthogonal Signal Division Multiplexing

Ebihara, Tadashi; Leus, Geert; Ogasawara, Hanako

DOI
10.1109/OCEANSKOBE.2018.8559404

Publication date
2018

Document Version
Final published version

Published in
2018 OCEANS - MTS/IEEE Kobe Techno-Oceans (OTO)

Underwater Acoustic Communication Using Multiple-Input Multiple-Output Doppler-Resilient Orthogonal Signal Division Multiplexing

Tadashi Ebihara
University of Tsukuba
Tsukuba, Japan

Geert Leus
Delft University of Technology
Delft, the Netherlands

Hanako Ogasawara
National Defense Academy
Yokosuka, Japan

***Abstract*—In this paper, we propose a novel underwater acoustic communication scheme that achieves energy and spectrum efficiency simultaneously by combining Doppler-resilient orthogonal signal division multiplexing (D-OSDM) and multiple-input multiple-output (MIMO) signaling. We present both the transmitter and receiver processing for MIMO D-OSDM. We evaluate the performance of MIMO D-OSDM in simulations with a large inter-symbol interference (60 symbols) and Doppler spread (maximum Doppler shift of 15 Hz). The simulation results show that MIMO D-OSDM achieves almost the same energy efficiency as normal D-OSDM while doubling the spectrum efficiency. We conclude that MIMO D-OSDM can become a viable technique that achieves reliable and effective UWA communication.**

***Keywords*—underwater acoustic communication, delay spread, Doppler spread, MIMO**

I. Introduction

Recently, underwater wireless communication systems have diversified dramatically. Multiple media (e.g., acoustic [1], [2], optical [3], and radio [4]) have been utilized to satisfy system requirements such as communication range and speed. Among these systems, underwater acoustic (UWA) communication offers wide area connectivity, since acoustic waves propagate over long distances in the underwater environment. On the other hand, UWA communication suffers from large delay and Doppler spreads of the UWA channel. To achieve reliable communication in such doubly spread channels, we have to spend more energy for channel sensing, resulting in low energy and spectrum efficiency.

To achieve reliable UWA communication, we have proposed Doppler-resilient orthogonal signal division multiplexing (D-OSDM) [5], [6]. D-OSDM is a communication technique for a single user and it is a combination of the OSDM [7] and orthogonal multiple access [8]; it places the pilot and data signals on a rectangular lattice in the time-frequency domain so that they do not interfere even in doubly spread channels. This signal structure enables the receiver to measure the delay-Doppler spread of the UWA channel efficiently, resulting in a reduction of the required transmission power. We have tested D-OSDM in simulations and test-tank experiments and have found that D-OSDM can reduce the power consumption requirements compared to the latest technique based on orthogonal frequency division multiplexing (OFDM). In addition, we have also conducted a demonstration of D-OSDM in a harbor with a mobile receiver, and confirmed that D-OSDM delivers excellent reliability in an actual UWA environment [9]. However, D-OSDM has a small spectrum efficiency, a limitation that should be addressed before we utilize this technique in an actual underwater application.

To achieve both energy- and spectrum-effective UWA communication, we combine single-user multiple-input multiple-output (MIMO) signaling and D-OSDM. Some initial works can be found in [10] and [11] but those papers focus on space-time or space-frequency coding. We instead use traditional MIMO signaling with different data streams on different antennas. We develop the transmitter and receiver processing for MIMO D-OSDM, and show that MIMO D-OSDM can improve the spectrum efficiency while preserving the characteristics of D-OSDM in terms of its resilience against delay and Doppler spreads. We also evaluate the performance of MIMO D-OSDM in doubly spread channels. Section II explains the signal processing flow of MIMO D-OSDM at the transmitter and receiver. Section III evaluates its performance in simulations. Section IV concludes this work.

II. MIMO D-OSDM

A. Signal Processing at the Transmitter

Fig. 1 shows the signal processing flow of MIMO D-OSDM at the transmitter and receiver. We assume that the transmitter and receiver employ J emitters and K hydrophones (J and K are positive integers and $J \leq K$). The transmitter reads a message and creates data matrices (DMs), $\boldsymbol{D}_0, \boldsymbol{D}_1 \ldots, \boldsymbol{D}_{J-1}$. Fig. 2 shows the structure of $\boldsymbol{D}_j$, where $\boldsymbol{p}_j$, $\boldsymbol{m}_{j,u,p}$, $\boldsymbol{0}_{2Q\times M}$ are a pilot signal of size $1\times M$, a message of size $1 \times M$ and a zeros matrix of size $2Q \times M$, respectively. Note that $j = 0, 1, \ldots, J-1$, $u = 0, 1, \ldots, U-1$, $p = 0, 1, \ldots, P-1$, and $N = 1 + 2Q + U(P + 2Q)$, where J, U, P, Q and M are positive integers. Q corresponds to the width of the Doppler spread of the UWA channel. Information about the pilot signal $\boldsymbol{p}_j$ is shared by both the transmitter and receiver prior to the communication. The transmitter then reads the DMs in a row-wise direction leading to data vectors of length MN, $\boldsymbol{d}_j$, and applies a transformation matrix to $\boldsymbol{d}_j$ to obtain a transmit signal $\boldsymbol{x}_j$ as follows:

$$\boldsymbol{x}_j = \boldsymbol{d}_j (\boldsymbol{F}_N \otimes \boldsymbol{I}_M), \tag{1}$$

where $\boldsymbol{F}_N$ and $\boldsymbol{I}_M$ are an inverse discrete Fourier transform (IDFT) matrix of size $N \times N$ and an identity matrix of size $M \times M$, respectively, and where "$\otimes$" represents the Kronecker product. Finally, the transmitter prepends L zeros to $\boldsymbol{x}_j$ ($L \leq M$

978-1-5386-1654-3/18/$31.00 ©2018 IEEE

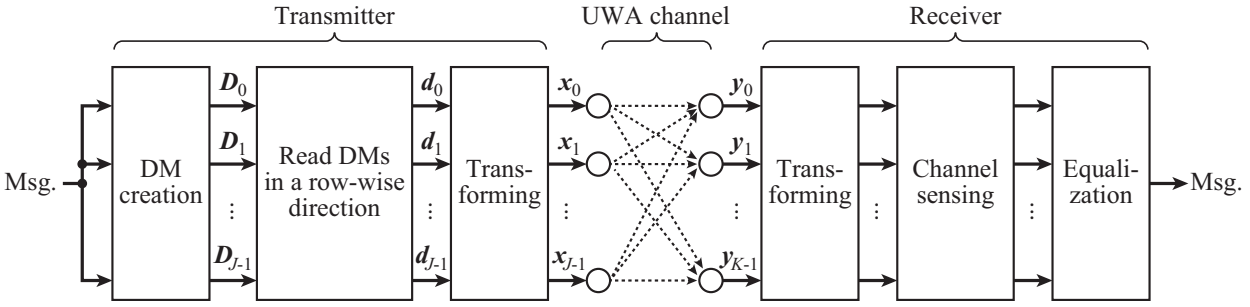

Fig. 1. Signal processing flow of MIMO D-OSDM at the transmitter and receiver.

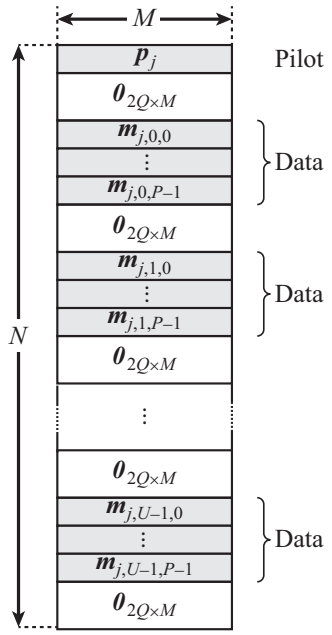

Fig. 2. Structure of data matrix, $\boldsymbol{D}_j$.

is a positive integer number that corresponds to the length of the delay spread of the UWA channel) and emits J zero-padded sequences simultaneously.

B. Signal Processing at the Receiver

The receiver receives K signals simultaneously and obtains sequences of length MN, $\boldsymbol{y}_k$ ($k = 0, 1, \ldots, K-1$), by an overlap-adding operation on each received signal. The obtained sequence can be expressed using a basis expansion model [12] as follows:

$$\boldsymbol{y}_k = \sum_{j=0}^{J-1} \left\{ \boldsymbol{x}_j \sum_{q=-Q}^{Q} \left(\boldsymbol{H}_q^{j\to k} \boldsymbol{\Lambda}_q \right) \right\} + \boldsymbol{\eta}_k. \tag{2}$$

In (2), $\boldsymbol{H}_q^{j\to k}$ is a circulant matrix,

$$\boldsymbol{H}_q^{j\to k} = \begin{pmatrix} h_{0,q}^{j\to k} & h_{1,q}^{j\to k} & \cdots & h_{MN-1,q}^{j\to k} \\ h_{MN-1,q}^{j\to k} & h_{0,q}^{j\to k} & \cdots & h_{MN-2,q}^{j\to k} \\ \vdots & \vdots & \ddots & \vdots \\ h_{1,q}^{j\to k} & h_{2,q}^{j\to k} & \cdots & h_{0,q}^{j\to k} \end{pmatrix}, \tag{3}$$

where $h_{m,q}^{j\to k}$ is the channel impulse response from emitter #j to hydrophone #k at Doppler scale q ($m = 0, 1, \ldots, MN-1$, and $h_{m,q}^{j\to k} = 0$ when $m > L$). Further, $\boldsymbol{\Lambda}_q$ is a diagonal matrix to represent the phase rotation at Doppler scale q,

$$\boldsymbol{\Lambda}_q = \begin{pmatrix} W_{MN}^{0} & 0 & \cdots & 0 \\ 0 & W_{MN}^{1} & \cdots & 0 \\ \vdots & \vdots & \ddots & \vdots \\ 0 & 0 & \cdots & W_{MN}^{(MN-1)q} \end{pmatrix}, \tag{4}$$

$$W_{MN} = \exp\left(\frac{2\pi\sqrt{-1}}{MN} \right). \tag{5}$$

Finally, $\boldsymbol{\eta}_k$ is the additive noise introduced at the receiver.

Now let us focus on the right-hand side of (2) (i.e., the part in curly brackets). If we apply a transformation matrix $\boldsymbol{F}_N^* \otimes \boldsymbol{I}_M$ to the part in curly brackets in (2), the output becomes (6) on the next page, where $\boldsymbol{C}^{j\to k}$ is a matrix of size $MN \times MN$,

$$\boldsymbol{C}^{j\to k} = \sum_{q=-Q}^{Q} \operatorname{diag}\left(\boldsymbol{C}_{0,q}^{j\to k}, \boldsymbol{C}_{1,q}^{j\to k}, \ldots, \boldsymbol{C}_{N-1,q}^{j\to k} \right) \boldsymbol{Z}_{MN}^{Mq}. \tag{7}$$

In (7), $\boldsymbol{C}_{n,q}^{j\to k}$ ($n = 0, 1, \ldots, N-1$) is a matrix of size $M \times M$,

$$\boldsymbol{C}_{n,q}^{j\to k} = \begin{pmatrix} h_{0,q}^{j\to k} & h_{1,q}^{j\to k} & \cdots & h_{M-1,q}^{j\to k} \\ W_N^{-n} h_{M-1,q}^{j\to k} & h_{0,q}^{j\to k} & \cdots & h_{M-2,q}^{j\to k} \\ \vdots & \vdots & \ddots & \vdots \\ W_N^{-n} h_{1,q}^{j\to k} & W_N^{-n} h_{2,q}^{j\to k} & \cdots & h_{0,q}^{j\to k} \end{pmatrix} \tag{8}$$

and $\boldsymbol{Z}_{MN}^{Mq}$ is a cyclic shift matrix of size $MN \times MN$,

$$\boldsymbol{Z}^{Mq} = \begin{pmatrix} 0 & 1 & 0 & \cdots & 0 \\ 0 & 0 & 1 & \cdots & 0 \\ \vdots & \vdots & \vdots & \ddots & 0 \\ 0 & 0 & 0 & \cdots & 1 \\ 1 & 0 & 0 & \cdots & 0 \end{pmatrix}. \tag{9}$$

$$\left\{\boldsymbol{x}_j \sum_{q=-Q}^{Q}\left(\boldsymbol{H}_q^{j\to k}\boldsymbol{\Lambda}_q\right)\right\}(\boldsymbol{F}_N^*\otimes\boldsymbol{I}_M) = \boldsymbol{d}_j(\boldsymbol{F}_N\otimes\boldsymbol{I}_M)\left(\boldsymbol{H}_q^{j\to k}\boldsymbol{\Lambda}_q\right)(\boldsymbol{F}_N^*\otimes\boldsymbol{I}_M) = \boldsymbol{d}_j\boldsymbol{C}^{j\to k}, \tag{6}$$

$$\begin{aligned}(\boldsymbol{z}_0,\boldsymbol{z}_1,\ldots,\boldsymbol{z}_{K-1}) &= (\boldsymbol{y}_0,\boldsymbol{y}_1,\ldots,\boldsymbol{y}_{K-1})\otimes(\boldsymbol{I}_K\otimes\boldsymbol{F}_N^*\otimes\boldsymbol{I}_M),\\ &= (\boldsymbol{d}_0,\boldsymbol{d}_1,\ldots,\boldsymbol{d}_{J-1})\begin{pmatrix}\boldsymbol{C}^{0\to0} & \boldsymbol{C}^{0\to1} & \cdots & \boldsymbol{C}^{0\to K-1}\\ \boldsymbol{C}^{1\to0} & \boldsymbol{C}^{1\to1} & \cdots & \boldsymbol{C}^{1\to K-1}\\ \vdots & \vdots & \ddots & \vdots\\ \boldsymbol{C}^{J-1\to0} & \boldsymbol{C}^{J-1\to1} & \cdots & \boldsymbol{C}^{J-1\to K-1}\end{pmatrix} + (\hat{\boldsymbol{\eta}}_0,\hat{\boldsymbol{\eta}}_1,\ldots,\hat{\boldsymbol{\eta}}_{K-1}),\end{aligned} \tag{11}$$

$$(\tilde{\boldsymbol{z}}_0,\tilde{\boldsymbol{z}}_1,\ldots,\tilde{\boldsymbol{z}}_{K-1}) = (\boldsymbol{p}_0,\boldsymbol{p}_1,\ldots,\boldsymbol{p}_{J-1})\begin{pmatrix}\tilde{\boldsymbol{C}}^{0\to0} & \tilde{\boldsymbol{C}}^{0\to1} & \cdots & \tilde{\boldsymbol{C}}^{0\to K-1}\\ \tilde{\boldsymbol{C}}^{1\to0} & \tilde{\boldsymbol{C}}^{1\to1} & \cdots & \tilde{\boldsymbol{C}}^{1\to K-1}\\ \vdots & \vdots & \ddots & \vdots\\ \tilde{\boldsymbol{C}}^{J-1\to0} & \tilde{\boldsymbol{C}}^{J-1\to1} & \cdots & \tilde{\boldsymbol{C}}^{J-1\to K-1}\end{pmatrix} + (\tilde{\boldsymbol{\eta}}_0,\tilde{\boldsymbol{\eta}}_1,\ldots,\tilde{\boldsymbol{\eta}}_{K-1}), \tag{14}$$

From (2) and (6), we have

$$\boldsymbol{y}_k(\boldsymbol{F}_N^*\otimes\boldsymbol{I}_M) = (\boldsymbol{d}_0,\boldsymbol{d}_1,\ldots,\boldsymbol{d}_{J-1})\begin{pmatrix}\boldsymbol{C}^{0\to k}\\ \boldsymbol{C}^{1\to k}\\ \vdots\\ \boldsymbol{C}^{J-1\to k}\end{pmatrix} + \boldsymbol{\eta}_k(\boldsymbol{F}_N^*\otimes\boldsymbol{I}_M). \tag{10}$$

Jointly handling all outputs, the receiver merges the $\boldsymbol{y}_k$ and applies a transformation matrix $\boldsymbol{I}_K\otimes\boldsymbol{F}_N^*\otimes\boldsymbol{I}_M$. The transformation output becomes (11), where

$$\hat{\boldsymbol{\eta}}_k = \boldsymbol{\eta}_k(\boldsymbol{F}_N^*\otimes\boldsymbol{I}_M). \tag{12}$$

Then the receiver performs channel sensing by extracting specific columns from $\boldsymbol{z}_k$ in (11) as

$$\tilde{\boldsymbol{z}}_k = (z_{k,0}, z_{k,1},\ldots,z_{k,M(1+Q)-1}, z_{k,N-MQ}, z_{k,N-MQ+2},\ldots,z_{k,N-1}), \tag{13}$$

where $\tilde{\boldsymbol{z}}_k$ is a vector of length $M(1+2Q)$ and $z_{k,n}$ is the n-th element of $\boldsymbol{z}_k$. In this case, there is a relationship among $\tilde{\boldsymbol{z}}_k$, $\boldsymbol{p}_j$ and $\boldsymbol{C}^{j\to k}$ as given in (14), where $\tilde{\boldsymbol{C}}^{j\to k}$ is a matrix of size $M\times M(1+2Q)$,

$$\tilde{\boldsymbol{C}}^{j\to k} = \left(\boldsymbol{C}_{0,-Q}^{j\to k}, \boldsymbol{C}_{0,-Q+1}^{j\to k},\ldots,\boldsymbol{C}_{0,Q}^{j\to k}\right), \tag{15}$$

and

$$\tilde{\boldsymbol{\eta}}_k = (\hat{\eta}_{k,0},\hat{\eta}_{k,1},\ldots,\hat{\eta}_{k,M(1+Q)-1},\hat{\eta}_{k,N-MQ},\hat{\eta}_{k,N-MQ+2},\ldots,\hat{\eta}_{k,N-1}), \tag{16}$$

with $\hat{\eta}_{k,n}$ the n-th element of $\hat{\boldsymbol{\eta}}_k$.

Hence, the receiver obtains $\boldsymbol{h}_q^{j\to k} = \left(h_{0,q}^{j\to k}, h_{1,q}^{j\to k},\ldots,h_{M-1,q}^{j\to k}\right)$ by solving (14) and obtaining $\tilde{\boldsymbol{C}}_{n,q}^{j\to k}$. Then the receiver calculates $\boldsymbol{C}_{n,q}^{j\to k}$ in (8) using $h_{m,q}^{j\to k}$, obtains $\boldsymbol{C}^{j\to k}$ in (7) by merging $\boldsymbol{C}_{n,q}^{j\to k}$ for all n, and successfully obtains $\boldsymbol{m}_{j,u,p}$ in $\boldsymbol{d}_j$ by solving (11).

The advantage of MIMO D-OSDM is an effective improvement of the spectrum efficiency; it can improve the spectrum efficiency J times that of normal D-OSDM while almost preserving its resilience against delay and Doppler spread. Note that the measurable delay spread of MIMO D-OSDM is $1/J$ times that of normal D-OSDM, because all J pilot signals interfere in MIMO D-OSDM. Specifically, MIMO D-OSDM measures $h_{m,q}^{j\to k}$ for $0\le m\le M/J$ and assumes $h_{m,q}^{j\to k}=0$ for $m>M/J$. This is because the receiver has to calculate $JK(2Q+1)$ channel impulse responses ($\boldsymbol{h}_q^{j\to k}$) from $(\tilde{\boldsymbol{z}}_0,\tilde{\boldsymbol{z}}_1,\ldots,\tilde{\boldsymbol{z}}_{K-1})$, whose length is $KM(1+2Q)$ by solving (14). However, in the next section, we show that the advantages of MIMO D-OSDM outweigh its disadvantages.

TABLE I. Parameters of MIMO D-OSDM and Normal D-OSDM Used in the Simulations.

	MIMO D-OSDM	Normal OSDM
M	63	
P	1	
Q	1	
U	1	
L	63	
J	2	1
K	2	2
Modulation	QPSK	QPSK / 16QAM
Channel coding	Turbo code (rate 0.5)	
Carrier frequency	35 kHz	
Signal bandwidth	3.6 kHz	
Effective data rate	1.0 kbps	0.5 / 1.0 kbps

III. Performance Evaluation

We evaluate the performance of MIMO D-OSDM in simulations. To show that MIMO D-OSDM can improve the spectrum efficiency effectively, we compare the performances of MIMO D-OSDM and normal D-OSDM under comparable environments. Table I shows the parameters used in the simulations. We compare MIMO D-OSDM with two emitters and hydrophones (2×2) to normal D-OSDM with a single emitter and two hydrophones (1×2). We set normal D-OSDM (QPSK) as a reference, and benchmark both normal D-OSDM

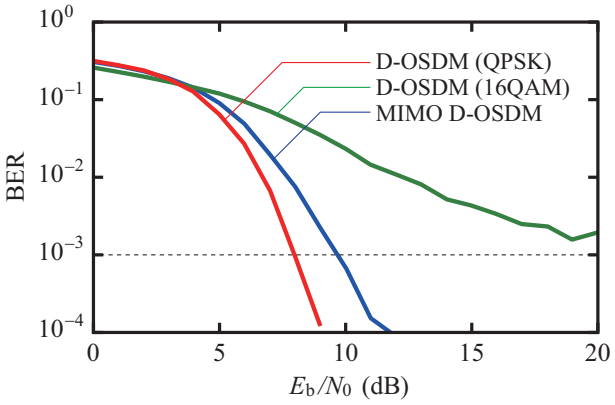

Fig. 3. Simulation results.

(16QAM) and MIMO-OSDM whose spectrum efficiencies are twice that of normal D-OSDM (QPSK).

To simulate a UWA channel with large delay and Doppler spreads, a discrete-time equivalent baseband channel model with a maximum delay of 60 taps (16 ms) and a maximum Doppler shift of 15 Hz was established. The channel was assumed to be a Rayleigh fading channel, and the gain of the discrete paths decreased 0.67 dB per tap in power. The channel impulse responses from emitter #j to hydrophone #k were assumed to be independent of each other. The Doppler spread was assumed to have a bell shape. By using this channel model, the relationship between E_b/N_0 and the bit error rate (BER) was investigated. Note that the total output power of the MIMO D-OSDM and normal D-OSDM transmitters is the same.

Fig. 3 shows the simulation results. The obtained results suggest that the MIMO technique can effectively improve the spectrum efficiency of D-OSDM. As shown in the figure, normal D-OSDM (QPSK) and MIMO D-OSDM achieve a BER of 10^{-3} when the E_b/N_0 is 8 and 9.6 dB, respectively. On the other hand, normal D-OSDM (16QAM) has a BER floor above 10^{-3}. This result shows that MIMO D-OSDM achieves almost the same performance as normal D-OSDM (QPSK) while doubling the spectrum efficiency. On the other hand, D-OSDM (16QAM) has an inferior performance, and the use of a higher modulation rate was less effective than the MIMO technique. As described above in Sec. II, the measurable delay spread of MIMO D-OSDM was limited compared to normal D-OSDM. Thus, there was a small difference between the performance of normal D-OSDM (QPSK) and that of MIMO D-OSDM. However, comparing MIMO D-OSDM and normal D-OSDM (16QAM) made it clear that the advantages of MIMO outweigh its disadvantages.

IV. Conclusion

In this study, we proposed MIMO D-OSDM to provide reliable and spectrum-effective UWA communication. We designed the signal processing to support multi-stream data transmission based on D-OSDM and evaluated its performance in simulations. We found that MIMO D-OSDM achieved almost the same performance as normal D-OSDM in a UWA channel whose delay and Doppler spreads were significant. The obtained results suggest that MIMO D-OSDM is a viable technique that achieves reliable and effective UWA communication. Experimental verification to support this simulation is one of the focus points of our future research.

Acknowledgments

This work was supported by Grant-in-Aid for Young Scientists (A), Japan Society for the Promotion of Science (15H05560).

References

[1] M. Stojanovic, "Recent advances in high-speed underwater acoustic communications," *IEEE Journal of Oceanic Engineering*, vol. 21, no. 2, pp. 125–136, Apr 1996.

[2] M. Chitre, S. Shahabudeen, and M. Stojanovic, "Underwater acoustic communications and networking: Recent advances and future challenges," *Marine Technology Society Journal*, vol. 42, pp. 103–116, 2008.

[3] Z. Zeng, S. Fu, H. Zhang, Y. Dong, and J. Cheng, "A survey of underwater optical wireless communications," *IEEE Communications Surveys Tutorials*, vol. 19, no. 1, pp. 204–238, Firstquarter 2017.

[4] X. Che, I. Wells, G. Dickers, P. Kear, and X. Gong, "Re-evaluation of rf electromagnetic communication in underwater sensor networks," *IEEE Communications Magazine*, vol. 48, no. 12, pp. 143–151, December 2010.

[5] T. Ebihara and G. Leus, "Underwater acoustic communication using doppler-resilient orthogonal signal division multiplexing," in *OCEANS 2014 - TAIPEI*, April 2014, pp. 1–4.

[6] ——, "Doppler-resilient orthogonal signal-division multiplexing for underwater acoustic communication," *IEEE Journal of Oceanic Engineering*, vol. 41, no. 2, pp. 408–427, Apr. 2016.

[7] T. Ebihara and K. Mizutani, "Underwater acoustic communication with an orthogonal signal division multiplexing scheme in doubly spread channels," *IEEE Journal of Oceanic Engineering*, vol. 39, no. 1, pp. 47–58, Jan 2014.

[8] G. Leus, S. Zhou, and G. B. Giannakis, "Orthogonal multiple access over time- and frequency-selective channels," *IEEE Transactions on Information Theory*, vol. 49, no. 8, pp. 1942–1950, Aug 2003.

[9] T. Ebihara, G. Leus, and H. Ogasawara, "Underwater acoustic communication using doppler-resilient orthogonal signal division multiplexing in a harbor environment," *Physical Communication*, vol. 27, pp. 24 – 35, 2018. [Online]. Available: http://www.sciencedirect.com/science/article/pii/S1874490717301052

[10] J. Han, W. Shi, and G. Leus, "Space-frequency coded orthogonal signal-division multiplexing over underwater acoustic channels," *The Journal of the Acoustical Society of America*, vol. 141, no. 6, pp. EL513–EL518, 2017. [Online]. Available: https://doi.org/10.1121/1.4983632

[11] J. Han and G. Leus, "Space-time and space-frequency block coded vector OFDM modulation," *IEEE Communications Letters*, vol. 21, no. 1, pp. 204–207, Jan 2017.

[12] F. Qu and L. Yang, "Basis expansion model for underwater acoustic channels?" in *OCEANS 2008*, Sept 2008, pp. 1–7.